Lysine 152 of MuLV Reverse Transcriptase Is Required for the Integrity of the Active Site†

Qingli Shi,‡ Kamalendra Singh,‡ Aashish Srivastava, Neerja Kaushik, and Mukund J. Modak*

Department of Biochemistry and Molecular Biology, University of Medicine and Dentistry of New Jersey Medical School, Newark, New Jersey 07103

Received March 19, 2002; Revised Manuscript Received September 30, 2002

ABSTRACT: Comparison of the three-dimensional structure of the active sites of MuLV and HIV-1 reverse transcriptases shows the presence of a lysine residue (K152) in the substrate-binding region in MuLV RT, while its equivalent position in HIV-1 RT is occupied by a glycine (G112). To investigate the role of K152 in the mechanism of the polymerase reaction catalyzed by MuLV RT, four mutant RTs, namely, K152A, K152R, K152E, and K152G, were generated and biochemically characterized. All muteins exhibited reduced polymerase activity on both RNA and DNA template-primers with K152E being the most defective. The template-primer binding affinity and the processivity of DNA synthesis, however, remained unchanged. The steady-state kinetic characterization showed little change in $K_{m\cdot dNTP}$ (except for that of K152E) and an ∼3−10-fold decrease in k_{cat} depending upon the template-primer and mutational substitutions. The ddNTP resistance patterns were unchanged for all muteins, suggesting no participation of K152 in ddNTP recognition. The ability of individual muteins to add dNTP on the covalently cross-linked enzyme−template-primer complex was significantly decreased. These results together with the analysis of the ion pairs in the catalytic apparatus of MuLV RT suggest that K152 participates in maintaining the integrity of the active site of MuLV RT. Examination of the prepolymerase ternary complex formation showed that neither the wild type nor any of the K152 muteins of MuLV RT are capable of forming stable ternary complexes. This property is in contrast to that of HIV-1 RT, which readily forms stable ternary complexes under similar conditions. These results further indicate that the catalytic mechanism of MuLV RT is significantly different from that of HIV-1 RT, despite the presence of a number of conserved motifs and amino acid residues.

Reverse transcriptase (RT)[1] is an essential structural and functional component of all retroviruses. Due to similar catalytic mechanism and substrate requirements, RT has been classified as a member of the DNA polymerase family of enzymes (*1*−*3*). It catalyzes the synthesis of a double-stranded linear proviral DNA copy of the viral RNA genome, which later integrates into the host chromosome (*4*). Similar structural topology and the occurrence of certain conserved motifs in many DNA polymerases and RTs have suggested a common catalytic mechanism for these enzymes (*5*−*14*). Biochemical data generated using site-directed mutagenesis have confirmed the catalytic importance of many conserved residues (*15*−*18*).

The primary sequence alignment of reverse transcriptases shows the presence of five highly conserved motifs (motifs A−E). Of these motifs, A and C appear to be universally conserved in all DNA polymerases. The occurrence of specific aspartate residues within motifs A and C serves as the identification tags. These carboxylate residues reside in the palm subdomain of RT and form divalent cation-mediated complexes with the substrate dNTP (*14*).

Despite the common and conserved architecture of the polymerase active site of HIV-1 and MuLV reverse transcriptases, experimental data indicate that some functional differences exist between these two enzymes. One of the intriguing differences is the dideoxynucleotide sensitivity of two enzymes. HIV-1 RT readily recognizes and incorporates dideoxynucleotides, whereas MuLV RT is significantly less sensitive to dideoxynucleotides (*2*, *19*−*21*). In addition, Halvas et al. (*19*) have shown that both the wild-type (WT) and V223M mutant of MuLV RT retain resistance to 2′,3′-dideoxy-3′-thiacytidine (3TC). Other examples are the functional roles of Q151 and Y183 of HIV-1 RT and their equivalent residues in MuLV RT (Q190 and Y222, respectively). Substitution of Q with A in both enzymes results in the inactive phenotypes (*19*, *23*); however, substitution of

† Supported in part by a grant from the National Institute of General Medical Sciences (GM 36307).

* To whom correspondence should be addressed: UMD-New Jersey Medical School, 185 S. Orange Ave., Newark, NJ 07103. Phone: (973) 972-5515. Fax: (973) 972-5594. E-mail: modak@umdnj.edu.

‡ These authors contributed equally to this work.

[1] Abbreviations: HIV-1, human immunodeficiency virus type 1; RT, reverse transcriptase; ddNTPs, dideoxyribonucleotides; MuLV, Moloney murine leukemia virus; WT, wild type; TP, template-primer; PP_i, pyrophosphate; PDB, Protein Data Bank; SDS−PAGE, sodium dodecyl sulfate−polyacrylamide gel electrophoresis; DTT, dithiothreitol; IPTG, isopropyl β-D-thiogalactopyranoside; IMAC, immobilized metal affinity chromatography; PSM, protein solubilizing medium; poly(rA)-$(dT)_{18}$, poly(riboadenylic acid) annealed with $(oligodeoxythymidylic\ acid)_{18}$; dNTP, deoxyribonucleoside triphosphate; dATP, dGTP, dCTP, and dTTP, nucleoside triphosphates of deoxyadenosine, deoxyguanosine, deoxycytidine, and thymidine, respectively; MS2 RNA, phage MS2 genomic RNA (single-stranded); U5-PBS RNA template, HIV-1 genomic RNA template corresponding to the primer binding sequence region; PBS, primer binding site.

10.1021/bi0258389 CCC: $22.00
Published on Web 11/20/2002

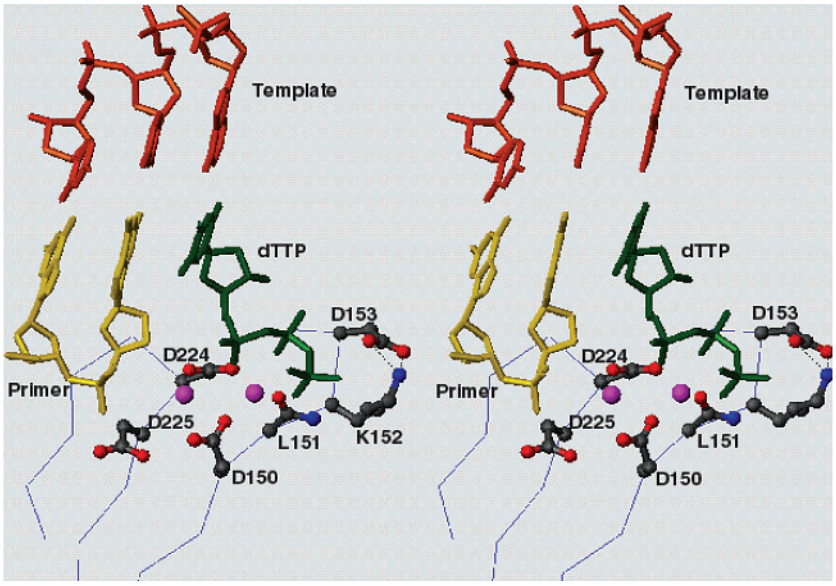

FIGURE 1: Stereoview of the active site of the modeled ternary complex of MuLV RT. This figure shows a close-up view of the active site of the modeled ternary complex using the ternary complex crystal structure of HIV-1 RT [PDB entry 1rtd (*26*)] and the N-terminal fragment crystal structure of MuLV RT [PDB entry 1mml (*12*)]. The template (brown), primer (yellow), and dNTP (green) together with four carboxylates and K152 (protein side chains are colored with C in gray, O in red, and N in blue) are shown. The Cα traces of β-strands 7, 10, and 11 are shown as blue lines. The salt bridge between K152 and D153 is represented with dotted lines. This salt bridge does not exist in HIV-1 RT due to the presence of a Gly residue at a position (112) equivalent to K152.

Q151 with N in HIV-1 RT yields a fully active enzyme (*23*). In contrast, the mutation of the equivalent residue **(**Q190) in MuLV RT (Q190N) results in a nearly complete loss of polymerase activity (*19*). Nevertheless**,** mutation of Q190 of MuLV RT to N190 alters dideoxynucleotide resistance in MuLV RT. Dideoxynucleotide selection by the Q190N mutant is approximately 7-fold greater than by WT MuLV RT (*21*). Similarly, substitution of Y183 with F in HIV-1 RT results in a significant loss of catalytic activity (*24*), while an identical substitution of Y222 of MuLV RT (Y222F) preserves full activity (*25*).

In this communication, the results of our continuing analysis of the active site of MuLV RT are reported. For this study, using catalytic carboxylates as the reference points, a comparison of the active site structures of MuLV RT and HIV-1 RT (Figure 1) was performed. In the structural comparison, we used the HIV-1 RT crystal structure complexed with the template-primer and dNTP (*26*) and superimposed the structure of N-terminal fragment of MuLV RT that has been crystallized by Georgiadis et al. (*12*). It is relevant to point out that the catalytic activity of this N-terminal fragment is extremely low. This is most likely due to the absence of a thumb region as well as other structural units of the enzyme. However, the overall geometry of this fragment of MuLV RT is remarkably similar to the corresponding section of HIV-1 RT. The N-terminal fragment of MuLV RT contains important functional domains, namely, the fingers and the palm. When these structural units of MuLV RT (*12*) were superimposed on the corresponding units from HIV-1 RT (*13*), the root-mean-square deviation between the Cα positions of the palm and fingers subdomains was 0.6−1.4 and for fingers domain was 0.6−1.7 Å. With respect to the background of these similarities, the presence of lysine at position 152 of MuLV RT appeared to be rather intriguing. In HIV-1 RT, the K152 equivalent position is occupied by a Gly (G112) and the adjacent D113 was seen to interact with incoming dNTP through its main chain N atom (*26*). Because of the location of K152 in the vicinity of the putative substrate binding pocket and because of its positively charged character, we suspected that K152 is likely to participate in the recognition and binding of the substrate dNTP and possibly the exclusion of ddNTP analogues by MuLV RT.

To understand the functional contribution of K152 of MuLV RT, we used site-directed mutagenesis and generated four substitutions as follows: (i) K152 to R152, a conserved substitution, (ii) K152 to A152, representing a nonconserved substitution, (iii) K152 to E152, introducing a negative charge at this position, and (iv) K152 to G152, a change that mimics an HIV-1 RT-like environment. The comparative biochemical analysis of the properties of the individual mutant proteins (muteins) was then carried out. Our results indicate that substitution of K152 with Ala, Gly, or Arg resulted in an enzyme species that was moderately deficient in its catalytic activity, while the serious defect was noted with the K → E substitution. The dideoxynucleotide resistance of the mutant MuLV RT proteins was unchanged, suggesting that K152 is not involved in the dideoxynucleotide resistance center. No major defects in $K_{m\cdot dNTP}$, $K_{D\cdot DNA}$, or processivity of DNA synthesis were noted for three of four muteins. The ion pair distribution pattern implies that K152 is responsible for maintaining the overall geometry of the active center. Interestingly, we noted that the template-primer binding affinities of HIV-1 RT and MuLV RT are vastly different. HIV-1 RT shows ∼50-fold greater affinity for both RNA and DNA template-primers than MuLV RT. Interestingly, MuLV RT failed to form a stable ternary complex unlike HIV-1 RT, which readily forms a very stable ternary complex. These results strongly suggest that despite the anatomical similarity of the catalytic pocket and the presence of conserved residues in the two RTs, the catalytic mechanisms of the two RTs are different.

EXPERIMENTAL PROCEDURES

Materials

Restriction and DNA-modifying enzymes were purchased from Promega, Boehringer Mannheim, or Stratagene. HPLC-purified dNTPs were from Boehringer Mannheim. Expression vector pET28a and *Escherichia coli* expression strain BL21 (pLysS) were obtained from Novagen. The QIAprep miniprep kit was from Qiagen. Radioactive dNTPs were purchased from NEN Life Science Products. Poly(rA) (∼300−350 nucleotides long) was purchased from P-L Biochemicals, Inc. Other oligo primers were synthesized at the Molecular Biology Resource Facility at the New Jersey Medical School. Fast flow chelating Sepharose for immobilized metal affinity chromatography (IMAC) was purchased from Pharmacia. All other chemical reagents were of the highest grade and were from Fisher, Millipore Corp., Boehringer Mannheim, and Bio-Rad.

Methods

Site-Directed Mutagenesis. In vitro site-directed mutagenesis of desired residues in MuLV RT was carried out by employing the QuickChange site-directed mutagenesis protocol of Stratagene Corp. (*27*). The desired mutation was introduced into the wild-type MuLV RT gene using sense and antisense mutant primers. The *Dpn*I-digested PCR product was then transformed into competent DH5α cells. The colonies that appeared in the LB-kanamycin (LB-Kan) plates were individually grown in LB-Kan medium at 37 °C overnight. The positive clones were confirmed by sequencing using Sanger's dideoxy termination method (*28*). The pET28a plasmid carrying the desired mutagenic change in the MuLV RT gene was transformed into *E. coli* expression strain BL21 (pLysS) for high-level expression.

Expression and Purification of Muteins. Expression and purification of the muteins were carried out with slight modification of the procedure described previously (*18*). Briefly, 5 mL of the overnight cell culture was transferred to 500 mL of LB-Kan medium, and cultures were incubated at 37 °C with shaking until the OD_{595} reached 0.3. Induction of the enzyme was carried out by addition of 100 μM IPTG followed by incubation at 30 °C for 4 h. Cells were harvested by centrifugation at 8000 rpm and 4 °C for 15 min, and the pellets were washed by suspending them in buffer containing 0.2 M NaCl and 10 mM Tris-HCl (pH 8.0). The cell pellet was resuspended in (4 mL/g wet weight of cells) lysis buffer [50 mM Tris-HCl (pH 7.8), 500 mM NaCl, 1 mM PMSF, 0.1% NP40, 10% sucrose, and 0.2% lysozyme] by stirring it gently on ice for 30 min followed by sonication (three times for 20 s at 50% of the total output). The extracts prepared in this manner were clarified by centrifugation at 15 000 rpm and 4 °C for 40 min. The supernatant was then diluted 2.5-fold with dilution buffer (50 mM Tris-HCl, 1 mM PMSF, and 10% sucrose), and streptomycin sulfate was added to a final concentration of 4% to precipitate the cellular DNA. After centrifugation for 30 min (15 000 rpm and 4 °C), the supernatant was applied to an IMAC column pre-equilibrated with buffer A [20 mM Tris-HCl (pH 7.5), 500 mM NaCl, and 5 mM imidazole]. The column was washed with 60 mL of buffer A followed by 30 mL of buffer A containing 75 mM imidazole. Finally, MuLV RT mutein was eluted with 300 mM imidazole in buffer A. Fractions containing the muteins were pooled and dialyzed against buffer B [50 mM Tris-HCl (pH 7.0), 100 mM NaCl, and 1 mM EDTA] at 4 °C followed by dialysis against buffer C [50 mM Tris-HCl (pH 7.0), 100 mM NaCl, 1 mM EDTA, and 50% glycerol]. The protein concentration was determined by the Bradford colorimetric assay (*28*), and the protein bands were visualized on an SDS−polyacrylamide gel.

Chart 1

Oligomeric template-primers.

MS2RNA/19C

19C primer: 5' CGT TAG CCA CTC CGA AGT G- 3'

MS2RNA template: 3' GCA AUC GGU GAG GCU UCA CGC AUA UUG CGC GUG CGG CCG CCU GAA…5'

26mer/18mer

26mer template: 3' GGC CGA TCA TCA TGA TCA TTG TCA TC 5'

18mer primer: 5' CCG GCT AGT AGT ACT AGT 3'

46mer/16mer

46mer template: 3' GCG CGG CTT AAG GGC GAT CGT TAT AAG ACG TCG GTT CGA AGG CGC G 5'

16mer primer: 5' CGC GCC GAA TTC CCG C 3'

30mer RNA/DNA (RNA/DNA hybrid for RNase H assay)

30 mer RNA template: 3' CAG GGA CAA GCC CGC GGU GAC GAU CUC UAA 5'

30 mer DNA primer: 5' GTC CCT GTT CGG GCG CCA CTG CTA GAG ATT 3'

33/21ddC

33mer template: 3'- GCA ATC GGT GAG GCT TCA CGG CAT ATT GCG GCT-5'

21mer primer: 5'- CGT TAG CCA CTC CGA AGT GC.ddC –3'(Last CMP is ddCMP)

21/13ddC and 21/10ddC template primers

21-mer template 3'- GCA ATC GGT GAG GCT TCA CGG – 5'

13-mer primer 5'- CGT TAG CCA CTC ddC – 3' (Last CMP is ddCMP)

10-mer primer 5' - CGT TAG CCA ddC – 3' (Last CMP is ddCMP)

DNA Polymerase Activity. The DNA polymerase activity assay of wild-type MuLV RT and its four muteins was carried out using a standard trichloroacetic acid precipitation assay (*29*). Homopolymeric poly(rA)-$(dT)_{18}$, poly(rC)-$(dG)_{18}$, and $(dC)_{60}$-$(dG)_{18}$ template-primers were used in this assay. The nucleotide molar ratio for these template-primers was 10:1. One hundred microliters of the reaction mixture contained 50 mM Tris-HCl (pH 7.8), 1 mM DTT, 0.01% BSA, 0.1% NP40, 150 nM template-primer, 20 μM dTTP or dGTP mixed with 0.5 μCi of [α-^{32}P]dTTP or -dGTP depending on the template-primer, 60 mM KCl, and 6−20 nM enzyme. Reactions were initiated by the addition of 5 mM $MgCl_2$ or 0.5 mM $MnCl_2$ [for poly(rA)-directed synthesis] followed by incubation at 37 °C for 10 min and quenched by the addition of 5% ice-cold TCA containing 10 mM $NaPP_i$. The acid precipitable DNA was collected on Whatman glass fiber filters and quantitated by liquid scintillation spectroscopy.

RNase H Activity. The RNase H activity of the WT and mutant proteins was determined to monitor if the overall folding pattern of the WT and K152 muteins of MuLV RT was similar and that the mutational site had no influence on RNase activity. A 30-mer RNA−DNA template-primer (Chart 1) was used as the RNase H substrate. The reaction mixture (5 μL) contained 50 mM Tris-HCl (pH 7.8), 10 mM DTT, 0.01% BSA, ∼10 nM ^{32}P-labeled RNA−DNA hybrid, 6.5 nM WT and mutein proteins, and 5 mM $MgCl_2$. The assay was carried out at room temperature for 15 min and

terminated by the addition of 4 μL of Sanger's gel loading buffer. The products were analyzed on a 12% polyacrylamide−urea gel followed by autoradiography on a PhosphorImager (Molecular Dynamics Inc.).

Pyrophosphorolysis Activity. The method used in this assay was slightly modified from a previously described method (*18*, *25*). The pyrophosphorolysis activity of the wild-type MuLV RT and the four muteins was measured by monitoring the reduction in the length of the 5′-^{32}P-labeled primer annealed to the template. The reaction mixture contained 50 mM Tris-HCl (pH 7.8), 1 mM DTT, 0.01% BSA, 60 mM KCl, 5 mM $MgCl_2$, 1 mM $NaPP_i$, 15 nM poly(rA)-$(dT)_{18}$ template-primer (primer dT_{18} was 5′-^{32}P-labeled), and 25 nM enzyme in a total volume of 5 μL. After incubation at 25 °C for 1 h, the reaction was stopped by the addition of 3 μL of Sanger's gel loading solution. The products were analyzed on a 12% polyacrylamide−urea denaturing gel followed by autoradiography on a Molecular Dynamics PhosphorImager.

Steady-State Kinetic Analyses. Determination of standard kinetic constants for various muteins was carried out on three homopolymeric poly(rA)-$(dT)_{18}$, poly(rC)-$(dG)_{18}$, and $(dC)_{60}$-$(dG)_{18}$ template-primers by the standard acid precipitation method. The primer extension assay was used for heteropolymeric MS2 RNA−19-mer template-primers as described above. Substrate dNTP concentrations in these experiments varied from 1 to 300 μM.

$K_{D\cdot DNA}$ Determination. To determine the affinity for binding of template-primer to the desired enzyme proteins, gel mobility shift assays were performed as previously described by Joyce and colleagues (*30*). Binding of 33/21-mer, a dideoxy-terminated template-primer (Chart 1), to various concentrations of enzyme was carried out in a buffer containing 50 mM Tris-HCl (pH 7.8), 5 mM Mg^{2+}, 10% (v/v) glycerol, and 0.1 mg/mL bovine serum albumin. The concentration of ^{32}P-labeled template-primer was 1000 pM. Ten different protein concentrations were used to bracket the $K_{D\cdot DNA}$ value. Samples were loaded on a 7% nondenaturing polyacrylamide gel. Separation of free template-primer from bound template-primer was effected by electrophoresis at 150 V for 80 min at 4 °C using 50 mM Tris-borate (pH 8). Gels were dried, then scanned in a PhosphorImager, and quantitated using ImageQuant software (Pharmacia).

Stable Ternary Complex Formation. Our method for assessing ternary complex formation is based on the procedure described by Scott and colleagues (*31*), where nondenaturing gel electrophoresis is used to identify the E·DNA·dNTP complex that represents the stable ternary complex. Briefly, in a final volume of 10 μL, the enzyme concentration capable of binding ~100% of template-primer was mixed with 5′-end-labeled dideoxynucleotide-terminated primer annealed to template (1000 pM 33/21-mer) in duplicate in a buffer containing 50 mM Tris-HCl (pH 7.8), 10% (v/v) glycerol, 5 mM Mg^{2+}, and 0.1 mg/mL bovine serum albumin. The E·DNA complexes were allowed to form on ice. To one of the duplicate samples cognate dNTP was added at a concentration of 200 μM to induce ternary complex formation. The stability of the E·DNA binary complex and the E·DNA·dNTP ternary complex was then assessed by the degree of persistence of the labeled template-primer in the E·DNA complex when challenged with a 500-fold excess of the same unlabeled template-primer. Under these conditions, a nearly complete dissociation of radiolabeled DNA occurs from the E·TP complex but not from the E·TP·dNTP ternary complex. Either HIV-1 RT or the Klenow fragment of *E. coli* DNA polymerase I was used as a positive control. All samples were resolved on a native 7% nondenaturing polyacrylamide gel, and the positions of the radioactive bands representing the E·DNA complex and free DNA were visualized by exposure to a PhosphorImager.

Assessment of Nucleotidyl Transferase Activity onto the Covalently Cross-Linked E·TP Complex. Nucleotidyl transferase activity was measured by monitoring the addition of a single nucleotide onto the enzyme−template-primer covalent complex (*32*, *33*). Briefly, the enzyme was cross-linked to a 26/18-mer DNA template-primer in a 50 μL reaction mixture containing 50 mM Tris-HCl (pH 7.8), 1 mM DTT, 5 mM $MgCl_2$, 500 nM enzyme, and 5 nM template-primer. The reaction mixture was then exposed to UV (wavelength of 254 nm) in a UV cross-linker at a dose of 3500 $\mu J/cm^2$. To determine the nucleotidyl transferase activity of the E·TP complex, the reaction mixture was adjusted to 0.5 M NaCl, followed by the addition of 1 μCi of complementary [α-^{32}P]dNTP. After incubation at 25 °C for 30 min, the reaction was terminated by the addition of SDS gel loading buffer, and an aliquot was analyzed on an 8% SDS−polyacrylamide gel. The incorporated nucleotide products by exposing the gel to PhosphoImager (Molecular Dynamics, a part of Pharmacia) and the radioactive bands were quantitated with ImageQuant software. The density of the radiolabeled band was then used to determine the extent of incorporation of the radioactive nucleotide per unit of protein for the individual reaction.

Processivity of DNA Synthesis. The mode of DNA synthesis by the WT and K152 muteins was determined with homopolymeric poly(rA)-$(dT)_{18}$ as well as heteropolymeric MS2 RNA-19-mer template-primers. Both primers were 5′-^{32}P-labeled and annealed with their corresponding templates in a 1:1 molar ratio. Five microliters of the reaction mixture contained 50 mM Tris-HCl (pH 7.8), 1 mM DTT, 5 mM $MgCl_2$ for MS2 RNA-19-mer or 0.5 mM $MnCl_2$ for poly-(rA)-$(dT)_{18}$, 60 mM KCl, 5 nM template-primer, 500 μM dTTP or a mixture of all four dNTPs, and 25 nM wild-type enzyme or the desired muteins (125 nM). Nonradioactive poly(rA)-$(dT)_{18}$ (in a 1:10 molar ratio) at a final concentration of 30 mM was used as the trap. The desired enzymes were incubated with the template-primer at 25 °C for 1 min followed by the addition of dTTP or dNTP together with the poly(rA)-$(dT)_{18}$ trap. Aliquots (5 μL) of the reaction mixture were then removed at 10 and 30 s, and mixed with Sanger's gel loading solution. The effectiveness of the trap was measured by inclusion of the trap together with the enzyme and the radioactive template-primer at 25 °C for 1 min followed by the addition of dTTP or dNTP substrate, and incubation was carried out for an additional 30 s. Unlimited synthesis was assessed by incubating the desired enzyme with the template-primer in the absence of the trap. The reaction products in all cases were separated on a 12% polyacrylamide gel and analyzed by autoradiography.

Determination of Monovalent and Divalent Cation Optima. Determination of the monovalent cation optima for the polymerase reaction by the individual enzyme was carried out by varying the KCl concentration between 0 and 200 mM using the standard polymerase assay with poly(rA)-(dT_{18}) as the template-primer and Mg^{2+} or Mn^{2+} as the

divalent cation. The enzyme concentration for WT was 6.5 nM, while that for muteins was 32.5 nM. The optimum concentration of Mg^{2+} and Mn^{2+} for the individual DNA polymerase activity was also determined in a similar manner by changing the final concentration of Mg^{2+} from 0.5 to 20 mM and that of Mn^{2+} from 0.25 to 2 mM.

Dideoxynucleotide (ddNTP) Sensitivity. The ddNTP sensitivity of muteins and WT was examined using MS2 RNA-19-mer template-primer in the presence of Mg^{2+}. The reaction mixture in a final volume of 5 μL contained 50 mM Tris-HCl (pH 7.8), 1 mM DTT, 0.01% BSA, ~2.5 nM template-primer, 6.5 nM WT (or 32.5 nM muteins to compensate for the low catalytic activity), 200 μM dNTP, 200 μM ddNTPs, and 5 mM $MgCl_2$. The reactions were carried out at 37 °C for 15 min and were terminated by the addition of 3 μL of Sanger's gel loading buffer. The products were resolved on a 12% polyacrylamide−urea gel followed by autoradiography on a PhosphorImager (Molecular Dynamics Inc.).

RESULTS

Site-Directed Mutagenesis and Purification of WT and K152 Muteins. To understand the participation of K152 of MuLV RT in the catalytic process, we generated four muteins, viz., K152E, K152A, K152R, and K152G, as described in Experimental Procedures and determined their properties. The WT and muteins were purified using the protocol described previously (*18*, *20*, *25*). The enzyme preparations were nearly homogeneous (>98% pure) as assessed by SDS−polyacrylamide gel analysis. The levels of protein expression, the overall yield, the solubility, and the chromatographic characteristics of the mutant proteins were similar to those of the WT enzyme, suggesting no significant change in the overall folding of the mutant enzymes. To further ensure that the mutant proteins have a folding pattern similar to that of WT, we assessed the RNase H activity of mutants and the WT protein. The RNase H activity was determined on a 30-mer RNA−DNA template-primer (Chart 1). The RNase H activity pattern of the WT and mutant enzymes was similar (data not shown). These results together with the similar $K_{D\cdot DNA}$ values (as described below) of WT and muteins suggest that the overall folding of the WT and K152 muteins of MuLV RT has remained unaltered.

DNA Polymerase Activity. The polymerase activity of WT and four muteins (K152E, K152A, K152R, and K152G) was assayed by acid precipitation of the products using three homopolymeric template-primers, namely, poly(rA)-$(dT)_{18}$, poly(rC)-$(dG)_{18}$, and $(dC)_{60}$-$(dG)_{18}$. The polymerase activity of muteins ranged from ~0.1 to 60% of the WT depending upon the template-primer and the substitution at K152. Replacement of Lys with Glu (K152E) showed the most severe loss of the polymerase activity with all three template-primers (Figure 2).

Pyrophosphorolysis Activity. Pyrophosphorolysis is considered the reverse of the polymerase reaction. We used homopolymeric poly(rA)-$(dT)_{18}$ template-primer to determine if the pyrophosphorolysis activity of the WT and muteins corresponds with the polymerase activity. Of the four muteins, K152E exhibited a nearly complete loss of pyrophosphorolysis activity in the presence of Mg^{2+}. This is consistent with the loss of its polymerase activity. The other three muteins (K152A, K152R, and K152G) exhibited greater pyrophosphorolysis activity than K152E but significantly less than that seen with the wild-type enzyme (Figure 3).

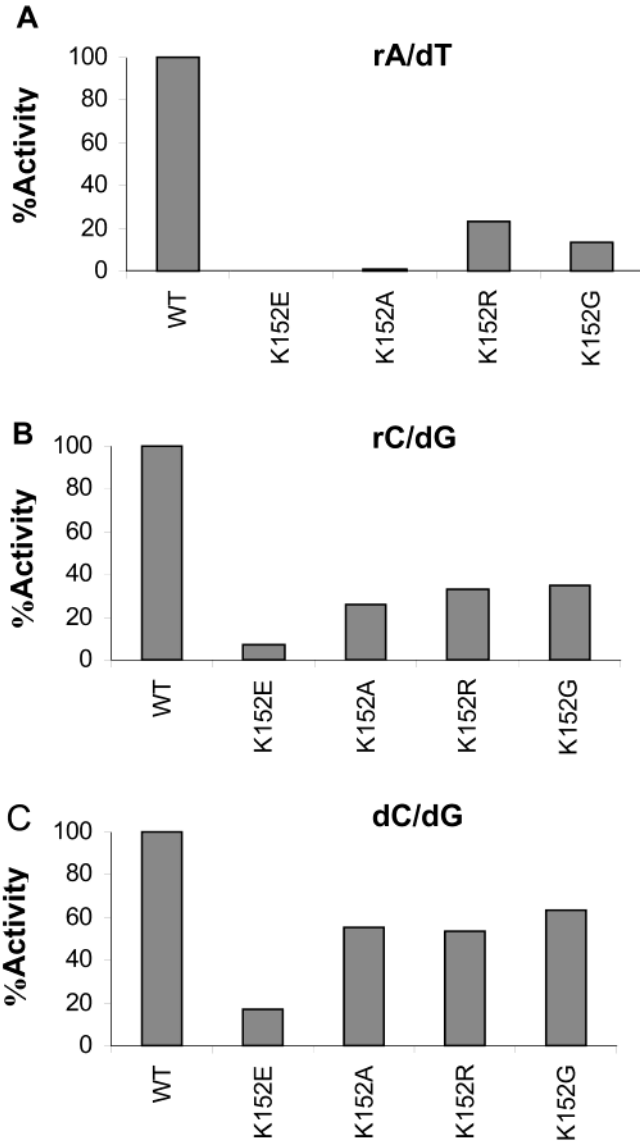

FIGURE 2: DNA polymerase activity of wild-type MuLV RT and its K152 mutant enzymes. A standard acid precipitation assay was used to examine the DNA polymerase activity of individual mutant enzymes on three homopolymeric poly(rA)-$(dT)_{18}$, poly(rC)-$(dG)_{18}$, and $(dC)_{60}$-$(dG)_{18}$ template-primers as described in Experimental Procedures. The activity of the wild-type enzyme was regarded as 100%. Activity values for the wild-type and mutant enzymes are averages of two independent experiments.

Dideoxynucleotide Resistance and Sensitivity. Since K152 is located in the putative substrate-binding pocket of MuLV RT, we had expected that the mutein at this site was likely to influence not only the substrate binding but also the resistance of WT MuLV RT to dideoxynucleotides. This expectation was based on the fact that HIV-1 RT, which exhibits good sensitivity to ddNTPs, has a Gly in place of Lys at the equivalent position in MuLV RT. It was therefore of interest to determine if any of the K152 muteins had acquired the ability to recognize ddNTP as judged by the ddNTP sensitivity. The results shown in Figure 4 clearly indicate that WT and all three muteins, including K152G (mimicking the HIV-1 RT environment), remain completely

Table 1: Steady-State Kinetic Parameters of WT and Mutant MuLV RTs on Various Template-Primers

enzyme	$K_{D\cdot DNA}$ (nM)[a]	poly(rA)-(dT)$_{18}$			poly(rC)-(dG)$_{18}$			poly(dC)-(dG)$_{18}$		
		K_m (μM)	k_{cat} (s^{-1})	k_{cat}/K_m (s^{-1} M^{-1})	K_m (μM)	k_{cat} (s^{-1})	k_{cat}/K_m (s^{-1} M^{-1})	K_m (μM)	k_{cat} (s^{-1})	k_{cat}/K_m (s^{-1} M^{-1})
WT	82	12	2	20×10^4	20	6×10^{-2}	29×10^2	4	3×10^{-2}	86×10^2
K152E	86	144	0.2	0.14×10^4	185	3×10^{-2}	1.5×10^2	35	0.3×10^{-2}	0.9×10^2
K152A	62	20	0.4	2.1×10^4	79	4×10^{-2}	4.6×10^2	21	1×10^{-2}	6.7×10^2
K152R	108	9	0.3	2.8×10^4	92	4×10^{-2}	4.4×10^2	15	1×10^{-2}	7.2×10^2
K152G	143	20	0.2	0.9×10^4	31	2×10^{-2}	7.7×10^2	8	0.4×10^{-2}	5.1×10^2

[a] The $K_{D\cdot DNA}$ values were estimated on a heteropolymeric 33/21-mer template-primer.

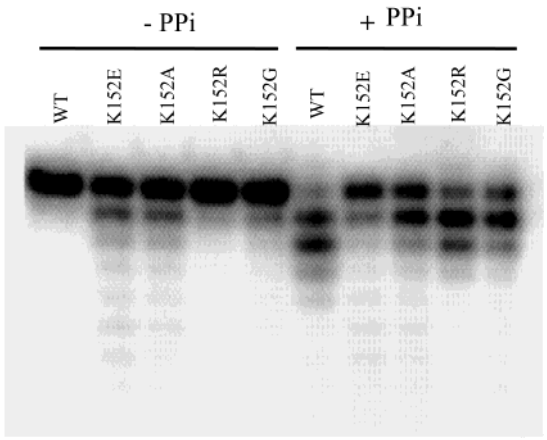

FIGURE 3: Pyrophosphorolysis activity of the wild-type and mutant enzymes. The pyrophosphorolysis activity of WT and mutant enzymes was assessed on a homopolymeric poly(rA)-(dT)$_{18}$ template-primer (1:1 molar ratio) as described in Experimental Procedures. The individual enzyme was incubated with the template-primer at room temperature for 1 h either in the absence ($-PP_i$) or in the presence ($+PP_i$) of 1 mM sodium pyrophosphate with 10 mM $MgCl_2$ followed by 12% polyacrylamide−urea gel electrophoresis. Note that the pyrophosphorolysis activity patterns of WT and the muteins correspond well with the polymerase activities of these enzymes. The WT enzyme shows maximum activity followed by K152R, K152G, K152A, and K152E.

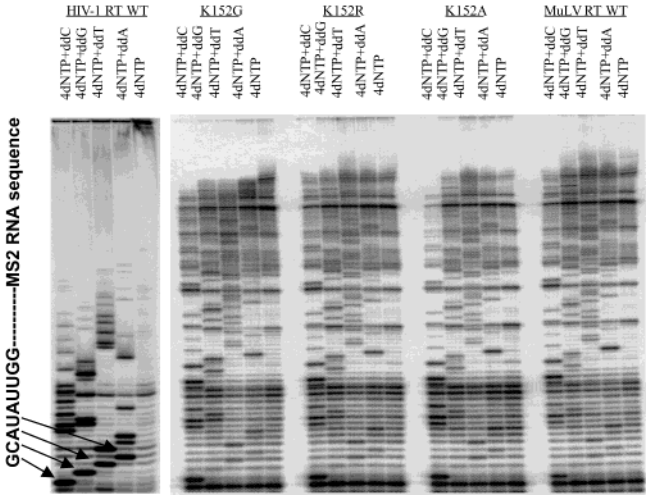

FIGURE 4: Dideoxynucleotide sensitivity of wild-type MuLV RT and its K152 muteins. The ddNTP sensitivity of the WT and K152 muteins was determined on MS2 RNA-19-mer DNA template-primer in the presence of $MgCl_2$ as described in Experimental Procedures. Lanes in all panels contained four dNTPs or four dNTPs with an individual ddNTP as marked at the top. The concentration of dNTPs and individual ddNTPs was 200 μM. Since wild-type HIV-1 RT is known to incorporate ddNTPs, it was used as a positive control. The figure clearly shows that the presence of ddNTPs in the reaction mixture did not alter the utilization of dNTP by wild-type and mutant MuLV RTs. In contrast, the distinct stops in the DNA products made by HIV-1 RT are clearly seen (indicated with arrows). Also shown on the left side is the initial sequence of the template region of MS2 RNA. The 3′-dideoxy-terminated products are not seen with WT and muteins of MuLV RT, suggesting that these enzyme species did not utilize dideoxynucleotides.

insensitive to ddNTP inhibition. The dideoxynucleotides incorporated by HIV-1 RT appeared in DNA products as strong stops (marked by arrows). In contrast, these stops were not visible in the product synthesized by MuLV RT and its three muteins (Figure 4).

Enzyme−Template-Primer Binding. The binding of the template-primer to an enzyme is the first step in the reaction pathway of DNA polymerases (*34*). To determine the effect of mutation of K152 on template-primer binding affinity, we determined the dissociation constant $K_{D\cdot DNA}$ for the WT MuLV RT, HIV-1 RT, and four muteins of MuLV RT with a gel shift assay. Results of these experiments are shown in Figure 5. The $K_{D\cdot DNA}$ was estimated by plotting the amount of E·DNA binary complex formed as a function of enzyme concentration. For the wild-type MuLV RT enzyme, the $K_{D\cdot DNA}$ for 33/21-mer template-primer was ~80 nM. The $K_{D\cdot DNA}$ values of muteins K152A, K152E, K152R, and K152G were 62, 86, 107, and 143 nM, respectively (Table 1). The comparison of $K_{D\cdot DNA}$ values of the WT and muteins shows that the affinity of K152G was decreased by ~2-fold. The other muteins (K152A, K152E, and K152R) had no significant alterations. Interestingly, the $K_{D\cdot DNA}$ for wild type HIV-1 RT was only ~2 nM for the same template-primer. These results suggested that HIV-1 RT binds to the template-primer with significantly higher affinity than does MuLV RT. Several crystal structures of MuLV RT bound to template-primers of various lengths have been reported (*35*, *36*). The DNA bound to MuLV RT in these structures contained duplexes of ~8−10 bp. Since the crystal structures represent a very stable state of the complex of DNA and MuLV RT, we also determined the affinity of the template-primer with MuLV RT using template-primers containing shorter duplexes (10- and 13-mer). We also included wild-type HIV-1 RT for comparison. To our surprise, the affinity of the wild-type MuLV RT did not change significantly from that obtained with 33/21-mer, whereas HIV-1 RT exhibited a significant loss in affinity for the template-primers containing a shorter duplex (Table 2).

Steady-State Kinetic Parameters. The steady-state kinetic parameters were determined to further clarify the role of Lys152 in the catalytic process. The kinetic parameters, K_m for dNTP utilization and k_{cat} for the polymerase reaction, were determined on three template-primers [poly(rC)-(dG)$_{18}$, poly(rA)-(dT)$_{18}$, and poly(dC$_{60}$)-(dG)$_{18}$]. The WT enzyme and muteins K152A, K152R, and K152G exhibited nearly identical $K_{m(dTTP)}$ values, whereas K152E showed an approximately 12-fold increase in $K_{m(dNTP)}$ (Table 1). Mutein

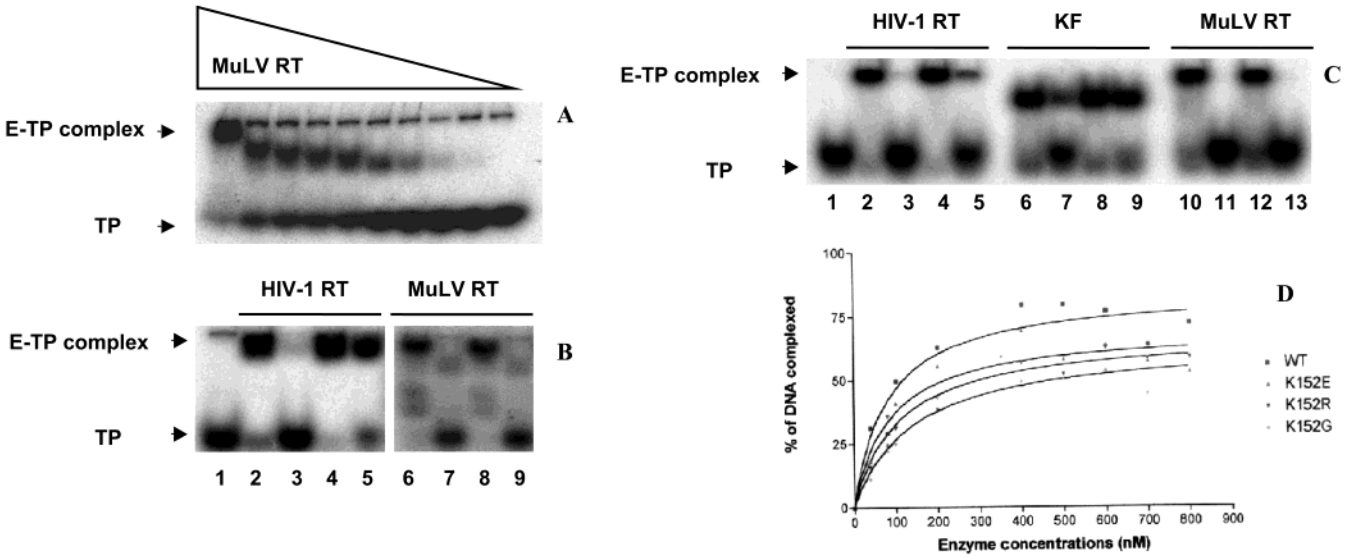

FIGURE 5: Enzyme−TP binding and the prepolymerase ternary complex as assessed by a gel shift assay. The 5′-^{32}P-labeled 21-mer primer was annealed to a 33-mer template in a 1:2.5 ratio followed by incubation of the template-primer (1000 pM) with wild-type MuLV RT (10−800 nM) on ice to form the E·TP complex. The template-primer binding pattern was resolved on a 6% polyacrylamide gel at 150 V for 1 h. A representative profile of template-primer binding to the WT enzyme is shown in panel A. The $K_{D\cdot DNA}$ was calculated by plotting bound template-primer against enzyme concentration and fitting the plot to the one-site binding (hyperbolic) curve. The curves obtained with individual muteins and WT MuLV RT are shown in panel D. In panel B, prepolymerase ternary complex formation by HIV-1 RT and MuLV RT is shown. In these experiments, 100 ng of MuLV RT was used in a reaction volume of 10 μL in each lane, whereas only 20 ng of WT HIV-1 RT was sufficient for both binary and ternary complexes. Lane 1 in this panel shows the amount of input template-primer. Lanes 2 and 6 show the binary complexes formed by HIV-1 RT and MuLV RT, respectively. The retention of bound radiolabeled species in the presence of a 500-fold excess of unlabeled template-primer is shown in lanes 3 and 7 for the two enzymes. The ternary complex formed in the presence of dNTP and the persistence of this complex after the addition of a 500-fold excess of template-primer are shown in lanes 4 and 5 for HIV-1 RT and 8 and 9 for MuLV RT, respectively. Note the retention of the complex in HIV-1 RT (lane 5) but not in MuLV RT (lane 9). Panel C shows the stable ternary complex formation by HIV-1 RT (left), the Klenow fragment (KF) of *E. coli* DNA polymerase I (middle), and MuLV RT (right) using a template-primer (21/13ddC) containing a shorter (13 bp) duplex region. The assay was performed in a manner similar to that used for panel B except that 100 ng of HIV-1 RT was used, since the binding affinity of this enzyme with 21/13ddC was reduced (Table 2). Lanes 2, 6, and 10 show the binary complex formed by HIV-1 RT, KF, and MuLV RT, respectively. The retention of bound radiolabeled species in the presence of a 500-fold excess of the unlabeled template-primer is shown in lanes 3, 7, and 11 for the three enzymes. The ternary complex formed in the presence of dNTP and the persistence of this complex after the addition of a 500-fold excess template-primer are shown in lanes 4 and 5 for HIV-1 RT, 8 and 9 for KF, and 12 and 13 for MuLV RT, respectively. Results clearly show that neither MuLV RT nor HIV-1 RT can form a stable ternary complex with a template-primer containing smaller (13 bp) double-stranded region. In contrast, KF readily forms a stable ternary complex with the 21/13ddC template-primer.

Table 2: Binding Affinities of Various DNA Polymerases with Template-Primers with Varying Duplex Lengths[a]

enzyme	template-primer	$K_{D\cdot DNA}$ (nM)
MuLV RT	33/21-mer	85
	21/13-mer	110
	21/10-mer	>260
HIV-1 RT	33/21-mer	2
	21/13-mer	80
	21/10-mer	>100
KF	33/21-mer	3
	21/13-mer	2
	21/10-mer	>50

[a] The binary complexes of enzymes with the desired template-primer containing a decreasing length of duplex region were formed with increasing concentrations of the indicated enzymes. The extent of the formation of the E·DNA complex was determined by a gel retardation assay (see Experimental Procedures). The $K_{D\cdot DNA}$ values for the individual enzyme proteins were determined by quantitating the complexes.

K152E also exhibited 12- and 27-fold increases in $K_{m(dNTP)}$ on heteropolymeric 26/18-mer and MS2 RNA-19-mer template-primers, respectively (data not shown). A nearly 5−10-fold decreased k_{cat} was noted for K152A, K152R, and K152G mutants on the poly(rA)-(dT)$_{18}$ template-primer. The catalytic efficiency of the muteins as judged by k_{cat}/K_m was significantly altered for only K152E. This mutant had ~100−150-fold decreased catalytic efficiency on all the template-primers that were used. The muteins K152A, K152G, and K152R exhibited ~4−20-fold decreases in the catalytic efficiency compared to that of WT (Table 1). The comparison of the catalytic efficiencies of the mutants on poly(rC)-(dG)$_{18}$ and poly(dC$_{60}$)-(dG)$_{18}$ showed that all muteins were slightly more deficient on poly(dC$_{60}$)-(dG)$_{18}$ than on poly(rC)-(dG)$_{18}$ (Table 1). These kinetic results were in contrast to initial activity data, which were obtained with a single substrate concentration.

Addition of dNTP onto the Enzyme−DNA Covalent Complex by Muteins. The $K_{D\cdot DNA}$ determination by gel shift assays showed that the mutation of K152 does not significantly alter the template-primer binding affinity. In addition, except for the K152E mutant, the K_m for dNTP utilization was not altered significantly. Therefore, to clarify if the net decrease in the catalytic efficiency of the mutants was possibly due to the alteration in the position of the template-primer, we used UV-mediated cross-linking of TP to the enzyme and assessed the ability of individual muteins to add dNTP onto the covalently bound template-primer. Two different template-primers (26/18-mer DNA and 30-mer RNA−19-mer DNA) were used for this experiment. The relative nucleotidyl transferase activity as judged by the addition of a single nucleotide of the individual mutein was

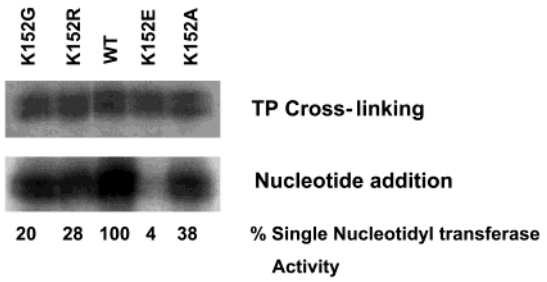

FIGURE 6: Enzyme−template-primer cross-linking and in situ nucleotide addition on the cross-linked template-primer: The UV-mediated photo-cross-linking of the 5′-^{32}P-labeled template-primer to the WT and mutant MuLV RT enzymes was performed as described in Experimental Procedures. The enzyme concentrations were normalized to obtain equal amounts of cross-linking. The cross-linking of template-primer is shown in panel A. In panel B, the results of single nucleotide addition in situ to the cross-linked template-primer to the enzyme are shown in the bottom panel. For this purpose, enzyme(s) and cold template-primer were exposed to UV radiation prior to addition of the radiolabeled [α-^{32}P]dNTP. To ensure nucleotide addition on only the cross-linked species, the salt concentration of the reaction mixture was adjusted to 500 mM. The amount of nucleotide addition shown under each lane was estimated by quantitation of the autoradiograph.

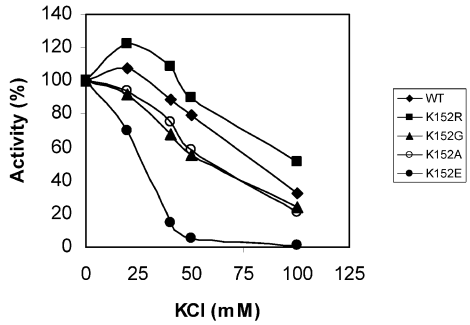

FIGURE 7: Salt tolerance by the WT and mutant MuLV RT enzymes. To assess the salt tolerance, the acid precipitation assays were performed at various KCl concentrations, using poly(rA)-$(dT)_{18}$ as the template-primer and Mg^{2+} as an effective divalent cation. The zero salt concentration in these assays is termed zero added salt. Note that the K152R mutant has greater salt tolerance than WT. The other muteins show progressively decreasing levels of DNA polymerization at increased KCl concentrations.

significantly lower than that seen with WT (Figure 6) and generally corresponded to the catalytic activity determined by acid precipitation assays (Figure 2). For the muteins K152E, K152G, K152R, and K152A, the activity was ∼4, ∼20, ∼28, and ∼38% of the WT activity, respectively.

Ternary Complex Formation by the Wild-Type and Mutant Enzymes. To obtain direct evidence of whether the dNTP binding in K152 muteins was altered, we examined the ability of each mutein to form a prepolymerase E·TP·dNTP ternary complex. Recently determined crystal structures of the ternary complexes of KlenTaq, T7 polymerase, and HIV-1 RT (*14*, *26*, *37*) have suggested that upon binding of the substrate dNTP to an E·DNA complex, rotational motion of the "fingers" domain occurs. This motion has been variously described as a "closed conformation" or closing of the nucleotide-binding site or "finger closing". An in vitro assay which represents this phenomenon has first been developed with HIV-I RT (in ref *31*, the authors refer to this as dead-end complex formation) and was later adapted for KF (*38*, *39*). We have also standardized this assay with KF and TB pol I to assess the ability of their muteins to form the ternary complex (*38*). As the template-primer used in these assays is terminated with ddNMP, the synthesis on the template-primer cannot occur. The results of this analysis for WT MuLV RT and HIV-1 RT are shown in Figure 5B. Lanes 1 and 6 show the E·DNA binary complex of wild-type HIV-1 RT and MuLV RT, respectively. The DNA in the binary complexes is readily competed out with excess unlabeled DNA as seen in lanes 2 and 5 (Figure 5B). It was interesting to point out that the $K_{D\cdot DNA}$ values for MuLV and HIV-1 RT differ significantly. The $K_{D\cdot DNA}$ for HIV-1 RT is ∼2 nM (Table 2), which is ∼40-fold lower that that seen for wild-type MuLV RT. When cognate nucleotide substrate is added to the E·DNA binary complex, a stable ternary complex is readily formed by HIV-1 RT as judged by the retention of labeled template-primer upon addition of challenge cold DNA (Figure 5B, lane 5). No such ternary complex is apparent, however, with both wild-type MuLV RT and its mutant derivatives (the data for muteins are not shown), as judged by the lability of the template-primer in the binary complex to the excess trap DNA, despite the presence of complementary nucleotide at high concentrations (Figure 5B, lane 9). Since template-primers containing shorter duplexes [∼10 bp were successfully crystallized with MuLV RT (*35*, *36*)], we examined their ability (despite rather suboptimal binding observed in our $K_{D\cdot DNA}$ determination; see Table 2) to form ternary complexes. With 21/13-mer and 21/10-mer template-primers, no ternary complex was apparent with MuLV RT or HIV-1 RT (Figure 5C) (the data for the 21/10-mer are not shown). In contrast, the Klenow fragment readily formed a ternary complex with the same template-primer.

Monovalent and Divalent Cation Optima for DNA Polymerase Activity. The crystal structures of the MuLV RT enzyme in the apo form show that K152 forms a salt bridge with D153, which is one of the conserved carboxylate residues. Therefore, we suspected that the mutation that disrupts this salt bridge might alter the optima or the sensitivity of the mutant enzymes to mono- and/or divalent cations. To investigate this possibility, we determined the optimal concentration of Mg^{2+}, Mn^{2+}, and KCl required for the catalytic activity of the WT and all muteins on the poly-(rA)-$(dT)_{18}$ template-primer.

The results indicated no change in the optimum concentration of both divalent cations required for the polymerase activity of all the enzyme species (data not shown), indicating that the metal coordination geometry at the active site has not been altered. However, with monovalent cations, muteins exhibited a somewhat altered sensitivity pattern, compared to that of the WT. The optimum activity for the WT and K152R MuLV RTs was at ∼20 mM KCl, whereas for the other three mutants (K152A, K152G, and K152E), the optimal activity was obtained without added KCl (Figure 7). In addition, the conserved K152R mutein showed a greater tolerance for the salt than did the WT. Furthermore, the nonconserved mutants (K152G, K152A, and K152E) have less tolerance for an increasing salt concentration. These results indicate that the salt bridge between K152 and D153 may be required for the optimal activity of MuLV RT.

Processivity of DNA Synthesis. The processivity of DNA synthesis was examined on the homopolymeric poly(rA)-$(dT)_{18}$ and heteropolymeric MS2 RNA-19-mer template-

primers r to determine whether the processivity of the DNA synthesis was affected due to the mutation at K152. Our results exhibited no significant defect in the processivity between the WT and the muteins with both template-primers (data not shown).

DISCUSSION

Comparison of DNA-bound HIV-1 RT structure (*10, 13*) with that of the N-terminal fragment of MuLV RT led Georgiadis et al. (*12*) to conclude that the active site architecture of the two enzymes is conserved. Several cocrystal structures of HIV-1 RT with NNRTI or DNA/dNTP were reported later, confirming similar domain arrangements and active site makeups of the two RTs (*12*, *13*, *26*). Despite the fact that the two enzymes have similar structures, they exhibit many biochemical differences. One of the major differences is the dideoxynucleotide sensitivity of the two enzymes; HIV-1 RT incorporates dideoxynucleotides much more efficiently (~1000-fold) than MuLV RT (*2*). In HIV-1 RT, M184 present in the YMDD motif has been shown to be partially responsible for AZTTP sensitivity (*40*). In MuLV RT, mutation of its YVDD motif to YMDD did not alter the nucleoside drug resistance properties of MuLV RT (*20*). Furthermore, both the wild type and the YMDD mutein of MuLV RT are also shown to be resistant to nucleoside analogue 3TC (*19*). The resistance of wild-type MuLV RT to dideoxynucleotides is also clear from Figure 4. The comparison of the ddNTP incorporation by HIV-1 RT with that of MuLV RT clearly indicates that while HIV-1 RT incorporated all four ddNTPs (ddCTP, ddGTP, ddTTP, and ddATP) in the DNA product, MuLV RT did not incorporate these substrates. To determine the contribution of various amino acids in the active site area and particularly the amino acids involved in the exclusion of ddNTP incorporation by MuLV RT, we carried out extensive structural analysis of the active sites of MuLV RT and HIV-1 RT. We focused our attention on the active site region in the two enzymes, which contained four catalytically important carboxylates contributed by motifs A and C (*5*).

Sequence alignment and structural comparison of motif A of HIV-1 RT and MuLV RT show that K152 of MuLV RT is not conserved throughout the RT family of DNA polymerases and is replaced with Gly in HIV-1 RT. The presence of this positively charged residue (K152) in the cluster of conserved carboxylates (D150, D153, D224, and D225) and the fact that the equivalent position in HIV-1 RT is occupied by G112 appeared to indicate some unique function for K152 in MuLV RT. In addition, in the three-dimensional structure of a fragment of MuLV RT (in the apo form; PDB entry 1MML**)**, this lysine forms a salt bridge with D153 (*12*). However, in the crystal structures of the N-terminal fragment of MuLV RT complexed with DNA, the orientation of the K152 side chain is such that it does not favor the hydrogen bond between K152 and D153 (PDB entries 1QAI, 1QAJ, and 1D1U). The ion pair formation can still be postulated if the putative change in the orientation of K152 side chain in the DNA-bound structure to that seen in the apo structure, upon binding of a dNTP substrate, has taken place. In HIV-1 RT, the position of K152 is occupied by a glycine (G112), which cannot form an ion pair. Nevertheless, D113 of HIV-1 RT makes contact with the β-phosphate of dNTP through its main chain (*26*). Considering these observations, we surmised that the participation of K152 of MuLV RT in the dNTP binding pocket would be different from that of G112 of HIV-1 RT. To gain some insight into the role of K152 of MuLV RT, we characterized four mutants of this residue and determined the biochemical properties of the mutant proteins. One of these mutants, K152G, was expected to mimic at least some properties of HIV-1 RT.

The polymerase activity of all muteins was observed to be lower than that of the WT, although the extent of activity reduction was dependent on the mutant and template-primer, suggesting that K152 is required for efficient DNA synthesis but is not absolutely essential. Initial examination showed that both the RNA and DNA-directed DNA synthesis were affected by mutation of K152 (Figure 2). The differential activity changes seen with K152 muteins could have serious functional consequences in vivo as seen with the D114 and R116 mutants of MuLV RT (*43*). To investigate the effect of the K152 mutation on template-primer binding, we determined the DNA binding affinity of the WT and four muteins with a gel mobility shift assay. The $K_{D\cdot DNA}$ (using 33/21-mer), determined from the gel mobility shift assays, ranged between 62 and 143 nM for the WT and muteins, suggesting modest differences in the DNA binding affinity. Therefore, the decrease in the catalytic activity of the muteins did not appear to result from the overall DNA binding defect. However, as the concentration of the enzyme was increased, a consistent shift in the position of the E·DNA complex was noted. Previously, it has been suggested (*41*, *42*) that MuLV RT binds the DNA in the dimeric form. The supershift seen here may be the result of homodimerization of the protein bound to the template-primer in this form.

As the examination of MuLV RT containing four different substitutions at the K152 site showed only a moderate loss of catalytic activity (with the exception of K152E) and a relatively small change in template-primer binding, we examined the ability of all four muteins to incorporate ddNTPs. Results showed that none of the K152 muteins show ddNTP recognition. Resistance to ddNTPs, as for WT MuLV RT, clearly indicates that K152 is not responsible for ddNTP discrimination by MuLV RT (Figure 4).

To further probe the reason for the decreased activity of the K152 muteins and to clarify the role for K152, we determined the steady-state kinetic parameters for the various muteins. These parameters (K_m for dNTP utilization and k_{cat} for polymerase reaction) are summarized in Table 1. Except for the K152E mutant, the change in K_m for three other muteins was 2−5-fold. Similarly, an ~5−10-fold change in k_{cat} as well as catalytic efficiency (k_{cat}/K_m) was noted with different template-primers with three muteins. For K152E, the reduction in efficiency was ~100−150-fold. The ability of an individual mutein to synthesize DNA in a processive manner also appeared to be unchanged despite the slow rate of catalysis (data not shown). These results suggest that impairment in the activity of muteins was not directly related to the binding of substrate or to the translocation involved in the polymerase reaction. Drastic effects seen with K152E may be attributed to the severe alteration of the local environment by the presence of an additional acidic residue at the active site, and therefore, results obtained with K152E may or may not be useful in deciphering the function of K152.

Since the three-dimensional structural data have indicated that K152 is located near the active center of MuLV RT and has the potential to form a salt bridge with the neighboring D153 during catalysis, it is possible that the substitution of K152 may subtly disturb the local geometry by not being able to form the ion pair with D153. This, in turn, may affect the binding of dNTP or the template-primer or alter the position of the template-primer at the active site. These two possibilities are ruled out since no significant difference in $K_{m\cdot dNTP}$ was seen and only a slight difference in DNA binding with various muteins of K152 was noted (Table 1). However, if we assume that K152, in addition to interacting with D153, interacts with the template-primer directly or indirectly (i.e., mediated by some other residue in the vicinity), alteration in the positioning of the template-primer as a function of altered active site geometry seemed plausible. To assess this possibility, we examined the ability of various muteins of K152 to catalyze the addition of a nucleotide onto the covalently cross-linked E·DNA complex. For this purpose, we carried out UV-mediated photo-cross-linking of various muteins to the template-primer and then determined the extent of incorporation of a single nucleotide onto the immobilized template-primer (*18*). The cross-linking site in the protein depends on the proximity of the bound DNA to that site. Cross-linking of TP to various muteins was found to be nearly identical (Figure 6). However, a subtle change in the position of the template-primer present in the individual E·TP complex was likely to be reflected in the efficiencies of the addition of a single nucleotide on the cross-linked template-primer. The extent of addition of a single nucleotide per unit of E−DNA covalent complex of individual muteins is given in Figure 6. Our results show that the extent of a single nucleotide addition corresponds well with the general activity patterns of the muteins. Therefore, it appears that the loss in the activity of the muteins has resulted from the alteration in the overall integrity of the active site. The processivity of the DNA synthesis by the WT as well as muteins was not changed. This suggests that once the template-primer binds to muteins, it does not dissociate from it prior to incorporating optimal numbers of nucleotides. The processivity data also suggest that the defect in the activity of the muteins is not due to the their inability to translocate along the template-primer. The reduction in the processivity of MuLV RT was reported by the mutation of its D114 and R116 (*43*). It is likely that the involvement of these two residues (D114 and R116) in the initial binding of the template-primer and processivity (*43*) is due to a salt bridge between them.

In this context, a salt bridge in the vicinity of the active center observed between K152 and D153 in both the apo (*12*) and the modeled ternary complex structures (*21*) indicated some functional utility. To examine the contribution of the ion pair between K152 and D153 at the structural level, we calculated the total number of ion pairs in the available crystal structures and in the model ternary complex of MuLV RT (*21*). The number of ion pairs was calculated by an in-house computer program (written in FORTRAN, available upon request) followed by their visualization using SYBYL (version 6.5, Tripos Associates, St. Louis, MO). RCSB (Research Collaboratory for Structural Bioinformatics, Rutgers University, New Brunswick, NJ) Protein Data Bank entry 1MML was used for salt bridge computations (*12*). A total of 15 ion pairs were found in the crystal structure of the apoenzyme (PDB entry 1MML). Five of these ion pairs were identified in the possible DNA-binding track, and the remaining 10 were distributed on the enzyme surface. Five ion pairs around the DNA-binding track are as follows: R116−D114, K120−E117, R121−E117, K152−D153, and K75−E176. Of these, only one (K152−D153) appeared to be in the vicinity of the primer terminus, while the other four are in the vicinity of the template strand. In this group, the R116−D114 ion pair is in the vicinity of the template nucleotide. Therefore, it appears that two ion pairs, one near the template (D114−R116) and the other near the primer (K152−D153), may be required for maintaining the proper orientation of the template-primer at the active site of MuLV RT. However, the deficiency in the processivity of DNA synthesis by the latter was not seen. It is possible that disturbance in the template-stabilizing ion pair would result in the loss of processivity as seen with R116−D114 muteins (*43*). To investigate if the ion pair between D153 and K152 plays a role in the efficient catalysis of nucleotide incorporation by MuLV RT, we assessed the alterations in the requirement for mono- and divalent cations for the activity of WT and its K152 muteins. Despite the lower activity of some of these muteins, the concentration of Mg^{2+} required for the optimal catalytic activity of WT and mutants remained unaltered. This result suggested that the disturbance in the metal−ligand geometry at the active site, which is essential for catalytic reaction, did not change due to the disturbance in the ion pair. This result also suggested that the salt bridge counterpart of K152, namely, D153, does not participate in metal chelation. In contrast, the activity response to various salt (monovalent cation) concentrations showed a small but consistent decrease in the activity of muteins**.** As shown in Figure 7, WT and K152R showed a greater tolerance for increased salt concentrations than K152G, K152A, and K152E muteins. These results further suggest a role for the ion pair between K152 and D153 in maintaining the integrity of the active site. To further clarify if the interaction between K152 and D153 is a salt bridge or hydrogen bond, we evaluated the activity of WT MuLV RT and its muteins at varying pHs ranging from 6.2 to 8.8. The pH optima and profile for the wild type and three of its muteins remained nearly constant (data not shown), suggesting that the mutational site (K152) does not participate via H-bonding. Since the activity profile in response to varying salt concentrations was different with individual muteins (Figure 7), the ion pair interaction between K152 and D153 seemed to be more important for the optimal functioning of MuLV RT.

The importance of salt bridges in the structure−function relationship of proteins has been extensively investigated. The formation of an ion pair between two oppositely charged residues has, for the most part, been associated with the stability of the protein structures. Vogt et al. (*44*) have analyzed the occurrence of salt bridges and hydrogen bonds in the structures of 16 protein families with different thermal stabilities. They observed a greater number of ion pairs in the proteins with higher thermostability. The importance of complex salt bridges (those joining more than two side chains) between charged protein residues has also been noted (*45*). Among their several observations, the most important was the role of complex salt bridges in connecting protein

subunits or joining the two secondary structures to form quaternary structures. The substrate binding and catalysis in lactose permease of *E. coli* have also been shown to be dependent on the ion pair found between its E126 and R144 (*46*). The muteins E126A and R144A did not bind the ligand or catalyze lactose accumulation, efflux exchange, downhill lactose translocation, or lactose-induced H^+ influx. A more closely related investigation pertaining to our study of the mutation of K152 is the mutational analysis of K143 located in the exonuclease domain of ϕ29 DNA polymerase (*47*). In the crystal structure of a related polymerase (T4 DNA polymerase) (*48*), the equivalent lysine residue (K299) forms a salt bridge with the conserved aspartate (D324). The catalytic importance of the aspartate residue has been shown in the exonucleolytic function of several DNA polymerases (*49*−*53*). The 3′−5′ exonuclease activity of ϕ29 DNA polymerase is also attributed to a salt bridge formed between its K143 and D169 (*47*).

Another pertinent example of the presence of an ion pair at the active site in the polymerases is the salt bridge between D192 and R258 of DNA polymerase β (*54*). Residue D192 of DNA polymerase β is an active site residue within conserved polymerase sequence motif C (*5*, *55*). The conservative mutation of this residue (D192E) eliminated the polymerase activity (*56*). Although the biochemical data suggest D192 is essential for catalysis, in the crystal structures of DNA pol β, the conformation of the side chain of this residue is variable and is not always poised for the catalytic process. When the thumb is closed, D192 serves as a ligand to dNTP-binding metal ion, as expected for the nucleotidyl transfer step. In contrast, when the thumb is open, D192 engages R258 via a salt bridge (*54*). On the basis of these two conformations of D192, the two functions of this active site aspartate have been proposed. First, in the closed conformation, the phenyl ring of F272 disrupts the salt bridge between D192 and R258, which frees D192 to ligate to the nucleotide-binding metal ion. Second, the closed conformation puts the side chain of thumb residues E295 and Y296 in position to form hydrogen bonds with R258, ensuring that R258 will not interfere with the ability of D192 to participate in catalysis (*54*). A complete demonstration of the events described above has been put together in the form of a movie available at http://chem-faculty.ucsd.edu/kraut/asp192.html. A similar situation can also be hypothesized for the presence of a salt bridge between K152 and D153 in MuLV RT. However, in the absence of additional structural data for MuLV RT complexes, the exact function of this salt bridge could not be assigned.

The presence of G112 in HIV-1 RT at a position equivalent to K152 of MuLV RT raises a question regarding the functionality of this residue (G112). No biochemical studies have yet been reported for muteins of G112. In the crystal structure of the ternary complex of HIV-1 RT containing the template-primer and dNTP, the main chain C═O group of G112 participates in the octahedral bipyramid coordination geometry of one of the two metals at the active site [structural metal (*57*, *58*)]. Since this interaction is common in the crystal structures of several DNA polymerase ternary complexes (*14*, *26*, *37*, *54*, *59*), no specific function can be ascribed to G112. However, the analysis of some crystal structures of HIV-1 RT [PDB entries 2HMI, 1RTD, and 1HYS (*13*, *26*, *60*)], a salt bridge is noted between D113 (D153 equivalent of MuLV RT) and K46. The position equivalent to K46 of HIV-1 RT in MuLV RT is occupied by I86. The function of this salt bridge (between K46 and D113 of HIV-1 RT) has not been established. It is possible that this salt bridge (present in HIV-1 RT) can serve a function analogous to that in MuLV RT (K152−D153). However, there appears to be a distinct difference between the two salt bridges described above, which may have functional significance. The ion pair in HIV-1 RT is between the residues present in two subdomains (D113 in the palm and K46 in the fingers), whereas the ion pair in MuLV RT is between the residues of the same (palm) subdomain. The salt bridge in HIV-1 RT may be hypothesized to play a role in stabilizing the formation of the ternary complex of HIV-1 RT. The absence in MuLV RT of an ion pair similar to that in HIV-1 RT between K46 and D113 may be one of the reasons that a stable ternary complex with MuLV RT (Figure 5) cannot be formed. In addition, as modeled in the above-mentioned crystal structures of HIV-1 RT, G112 has ϕ and ψ angles that are only permitted for a glycine residue and would be very high in energy for any other amino acid. These observations emphasize the fact that the architecture of the active site in two RTs (HIV-1 and MuLV) is somewhat different.

On the basis of the results of our extensive biochemical and structural analyses, we tentatively conclude that K152 contributes to the maintenance of the geometry of the active site required for the proper positioning of the template-primer in MuLV RT. In HIV-1 RT, the presence of Gly (G112) at the same topological position of K152 of MuLV RT implies yet another difference in the active site geometry.

REFERENCES

1. Baltimore, D. (1970) *Nature 226*, 1209−1211.
2. Skalka, A. M., and Goff, S. P. (1993) *Reverse transcriptase*, Cold Spring Harbor Laboratory Press, Plainview, NY.
3. Temin, H. M., and Mizutani, S. (1970) *Nature 226*, 1211−1213.
4. Gilboa, E., Mitra, S. W., Goff, S., and Baltimore, D. (1979) *Cell 18*, 93−100.
5. Delarue, M., Poch, O., Tordo, N., Moras, D., and Argos, P. (1990) *Protein Eng. 3*, 461−467.
6. Johnson, M. S., McClure, M. A., Feng, D. F., Gray, J., and Doolittle, R. F. (1986) *Proc. Natl. Acad. Sci. U.S.A. 83*, 7648−7652.
7. Xiong, Y., and Eickbush, T. H. (1990) *EMBO J. 9*, 3353−3362.
8. Kohlstaedt, L. A., Wang, J., Friedman, J. M., Rice, P. A., and Steitz, T. A. (1992) *Science 256*, 1783−1790.
9. Steitz, T. A., Smerdon, S., Jager, J., and Joyce, C. M. (1994) *Science 266*, 2022−2025.
10. Jacobo-Molina, A., Ding, J., Nanni, R. G., Clark, A. D., Lu, X., Tantillo, C., Williams, R. L., Kamer, G., Ferris, A. L., Clark, P., Hizi, A., Hughes, S. H., and Arnold, E. (1993) *Proc. Natl. Acad. Sci. U.S.A. 90*, 6320−6324.
11. Pelletier, H., Sawaya, M. R., Kumar, A., Wilson, S. H., and Kraut, J. (1994) *Science 264*, 1891−1903.
12. Georgiadis, M. M., Jassen, S. M., Ogata, C. M., Telesnitsky, A., Goff, S. P., and Hendrickson, W. A. (1995) *Structure 3*, 879−892.
13. Ding, J., Das, K., Hciou, Y., Sarafianos, S. G., Clark, A. D., Jr., Jacobo-Molina, A., Tantilo, C., Hughes, S. H., and Arnold, E. (1994) *J. Mol. Biol. 284*, 1095−1111.
14. Doublie, S., Tabor, S., Long, A. M., Richardson, C. C., and Ellenberger, T. (1998) *Nature 391*, 251−258.
15. Polesky, A. A., Dahlberg, M. E., Benkovic, S. J., Grindley, N. D., and Joyce, C. M. (1992) *J. Biol. Chem. 267*, 8417−8428.
16. Kaushik, N., Rege, N., Yadav, P. N. S., Sarafianos, S. G., Modak, M. J., and Pandey, V. N. (1996) *Biochemistry 35*, 11536−11546.
17. Pritchard, A. E., and McHenry, C. S. (1999) *J. Mol. Biol. 285*, 1067−1080.

18. Chowdhury, K., Kaushik, N., Pandey, V. N., and Modak, M. J. (1996) *Biochemistry 35*, 16610−16620.
19. Jin, J., Kaushik, N., Singh, K., and Modak, M. J. (1999) *J. Biol. Chem. 274*, 20861−20868.
20. Kaushik, N., Chowdhury, K., Pandey, V. N., and Modak, M. J. (2000) *Biochemistry 39*, 5155−5165.
21. Singh, K., Kaushik, N., Jin, J., Madhusudanan, M., and Modak, M. J. (2000) *Protein Eng. 13*, 635−643.
22. Halvas, K. H., Svarovskaia, E. S., Freed, E. O., and Pathak, V. K. (2000) *J. Virol. 74*, 6669−6674.
23. Harris, D., Yadav, P. N., and Pandey V. N. (1998) *Biochemistry 37*, 9630−9640.
24. Harris, D., Kaushik, N., Pandey, P. K., Yadav, P. N., and Pandey V. N. (1998) *J. Biol. Chem. 273*, 33624−33634.
25. Kaushik, N., Singh, K., Alluru, I., and Modak, M. J. (1999) *Biochemistry 38*, 2617−2627.
26. Huang, H., Chopra, R., Verdine, G. L., and Harrison, S. C. (1998) *Science 282*, 1969−1975.
27. Sambrook, J., Fritsch, E. F., and Maniatis, T. (1989) *Molecular Cloning: A Laboratory Manual*, 2nd ed., Cold Spring Harbor Laboratory Press, Plainview, NY.
28. Bradford, M. M. (1976) *Anal. Biochem. 72*, 248−254.
29. Modak, M. J., and Marcus, S. L. (1977) *J. Biol. Chem. 252*, 11−19.
30. Astatke, M., Grindley, N. D., and Joyce, C. M. (1995) *J. Biol. Chem. 270*, 1945−1954.
31. Tong, W., Lu, C., Sharma, S. K., Matsuura, S., So, A. G., and Scott, W. A. (1997) *Biochemistry 36*, 5749−5757.
32. Sarafianos, S. G., Pandey, V. N., Kaushik, N., and Modak, M. J. (1995) *Biochemistry 34*, 7207−7216.
33. Sarafianos, S. G., Pandey, V. N., Kaushik, N., and Modak, M. J. (1995) *J. Biol. Chem. 270*, 19729−19735.
34. Bryant, F. R., Johnson, K. A., and Benkovic, S. J. (1983) *Biochemistry 22*, 3537−3346.
35. Najmudin, S., Cole, M. L., Sun, D., Yohannan, S., Montano, S. P., Gu, J., and Georgiadis, M. M. (2000) *J. Mol. Biol. 296*, 613−632.
36. Cote, M. L., Yohannan, S. J., and Georgiadis, M. M. (2000) *Acta Crystallogr. D56*, 1120−1131.
37. Li, Y., Korolev, S., and Waksman, G. (1998) *EMBO J. 17*, 7514−7525.
38. Arrigo, C. J., Singh, K., and Modak, M. J. (2002) *J. Biol. Chem. 277*, 1653−1661.
39. Alekseyev, Y. O., Dzantiev, L., and Romano, L. J. (2001) *Biochemistry 40*, 2282−2290.
40. Hsu, M., Inouye, P., Rezende, L., Richard, N., Li, Z., Prasad, V. R., and Wainberg, M. A. (1997) *Nucleic Acids Res. 25*, 4532−4536.
41. Telensnitsky, A., and Goff, S. P. (1993) *Proc. Natl. Acad. Sci. U.S.A. 90*, 1276−1280.
42. Guo, J., Wu, W., Yuan, Z. Y., Post, K., Crouch, R. J., and Levin, J. G. (1995) *Biochemistry 34*, 5018−5029.
43. Gu, J., Villanueva, R. A., Snyder, C. S., Roth, M. J., and Georgiadis, M. M. (2001) *J. Mol. Biol. 305*, 341−359.
44. Vogt, G., Woell, S., and Argos, P. (1997) *J. Mol. Biol. 269*, 631−643.
45. Musafia, B., Buchner, V., and Arad, D. (1995) *J. Mol. Biol. 254*, 761−770.
46. Sahin-Toth, M., le Courte, J., Kharabi, D., le Marie, G., Lee, J. C., and Kabak, R. H. (1999) *Biochemistry 38*, 813−819.
47. de Vega, M., Ilyina, T., Lazaro, J. M., Salas, M., and Blanco, L. (1997) *J. Mol. Biol. 270*, 65−78.
48. Wang, J., Yu, P., Lin, T. C., Konigsberg, W. H., and Steitz, T. A. (1996) *Biochemistry 35*, 8110−8119.
49. Derbyshire, V., Freemont, P. S., Sanderson, M. R., Beese, L. S., Friedman, J. M., Joyce, C. M., and Steitz, T. A. (1991) *EMBO J. 10*, 17−25.
50. Esteban, J. A., Salas, M., and Blanco, L. (1993) *J. Biol. Chem. 268*, 2719−2726.
51. Reha-Krantz, L. J., and Nonay, R. L. (1993) *J. Biol. Chem. 268*, 27100−27108.
52. Ishino, Y., Iwasaki, H., Kato, I., and Shinagawa, H. (1994) *J. Biol. Chem. 269*, 14655−14660.
53. Foury, F., and Vanderstraeten, S. (1992) *EMBO J. 11*, 2717−2726.
54. Sawaya, M. R., Prasad, R., Wilson, S. H., Kraut, J., and Palletier, H. (1997) *Biochemistry 36*, 11205−11215.
55. Sawaya, M. R., Pelletier, H., Kumar, A., Wilson, S. H., and Kraut, J. (1994) *Science 264*, 1930−1935.
56. Date, T., Yamamoto, S., Tanihara, K., Nishimoto, Y., and Matsukage, A. (1991) *Biochemistry 30*, 5286−5292.
57. Steitz, T. A. (1998) *Nature 391*, 231−232.
58. Steitz, T. A. (1999) *J. Biol. Chem. 274*, 17395−17398.
59. Pelletier, H., Sawaya, M. R., Kumar, A., Wilson, S. H., and Kraut, J. (1994) *Science 264*, 1891−1903.
60. Sarafianos, S. G., Das, K., Tantillo, C., Clark, A. D., Jr., Ding, J., Whitcomb, J. M., Boyer, P. L., Hughes, S. H., and Arnold, E. (2001) *EMBO J. 20*, 1449−1461.

BI0258389